Interaction of Molecular Oxygen with the Vacuum-Annealed TiO 2 (110) Surface: Molecular and Dissociative Channels

ARTICLE · JUNE 1999

DOI: 10.1021/jp990655q

Interaction of Molecular Oxygen with the Vacuum-Annealed TiO_2(110) Surface: Molecular and Dissociative Channels

Michael A. Henderson,* William S. Epling,† Craig L. Perkins, and Charles H. F. Peden

Environmental Molecular Sciences Laboratory, Pacific Northwest National Laboratory, P.O. Box 999, MS K8-93, Richland, Washington 99352

Ulrike Diebold

Department of Physics, Tulane University, New Orleans, Louisiana 70118

Received: February 23, 1999; In Final Form: May 4, 1999

We have examined the interaction of molecular oxygen with the TiO_2(110) surface using temperature-programmed desorption (TPD), isotopic labeling studies, sticking probability measurements, and electron energy loss spectroscopy (ELS). Molecular oxygen does not adsorb on the TiO_2(110) surface in the temperature range between 100 and 300 K unless surface oxygen vacancy sites are present. These vacancy defects are generated by annealing the crystal at 850 K, and can be quantified reliably using water TPD. Adsorption of O_2 at 120 K on a TiO_2(110) surface with 8% oxygen vacancies (about 4×10^{13} sites/cm^2) occurs with an initial sticking probability of 0.5−0.6 that diminishes as the surface is saturated. The saturation coverage at 120 K, as estimated by TPD uptake measurements, is approximately three times the surface vacancy population. Coverage-dependent TPD shows little or no O_2 desorption below a coverage of 4×10^{13} molecules/cm^2 (the vacancy population), presumably due to dissociative filling of the vacancy sites in a 1:1 ratio. Above a coverage of 4×10^{13} molecules/cm^2, a first-order O_2 TPD peak appears at 410 K. Oxygen molecules in this peak do not scramble oxygen atoms with either the surface or with other coadsorbed oxygen molecules. Sequential exposures of $^{16}O_2$ and $^{18}O_2$ at 120 K indicate that each adsorbed O_2 molecule, irrespective of its adsorption sequence, has equivalent probabilities with respect to its neighbors to follow the two channels (molecular and dissociative), suggesting that O_2 adsorption is not only precursor-mediated, as the sticking probability measurements indicate, but that all O_2 molecules reside in this precursor state at 120 K. This precursor state may be associated with a weak 145 K O_2 TPD state observed at high O_2 exposures. ELS measurements suggest charge transfer from the surface to the O_2 molecule based on disappearance of the vacancy loss feature at 0.8 eV, and the appearance of a 2.8 eV loss that can be assigned to an adsorbed O_2^- species based on comparisons with Ti−O_2 inorganic complexes in the literature. Utilizing results from recent spin-polarized DFT calculations in the literature, we propose a model where three O_2 molecules are bound in the vicinity of each vacancy site at 120 K. For adsorption temperatures above 150 K, the dissociation channel completely dominates and the surface adsorbs oxygen in a 1:1 ratio with each vacancy site. ELS measurements indicate that the vacancies are filled, and the remaining oxygen adatom, which is apparent in TPD, is transparent in ELS. On the basis of the variety of oxygen adsorption states observed in this study, further work is needed in order to determine which oxygen-related species play important roles in chemical and photochemical oxidation processes on TiO_2 surfaces.

1. Introduction

The chemistry of O_2 is an important, but often overlooked, component of many chemical and photochemical processes that take place on TiO_2-based materials. Oxygen is widely used in photochemical oxidation studies on TiO_2 and is usually considered to act primarily as a scavanger of the photoexcited electrons, thus preventing negative charge accumulation on the catalyst particle.[1,2] In some solution-phase photochemical studies, the resulting O_2^- species are envisioned to participate in homogeneous-phase reactions with water molecules to form hydrogen peroxyl species that may perform organic oxidation, either in the solution or on the surface. Only a few groups have proposed that surface-bound O_2 or O_2^- species may be directly involved in photooxidation of coadsorbed species.[3] However, the exact nature of adsorbed O_2 on these TiO_2 surfaces is not well understood.

The thermal chemistry of O_2 on TiO_2 surfaces is also not well understood. Molecular oxygen is typically used by ultrahigh vacuum (UHV) researchers to restore the stoichiometry of ion-sputtered or vacuum-reduced TiO_2 surfaces. For example, Kurtz and co-workers have shown that surface defects generated on TiO_2(110) by high-temperature annealing are removed by O_2 exposure at 400 K.[4] This conclusion is consistent with low-energy ion scattering results by Pan et al. that show $^{18}O_2$ fills vacancy sites on TiO_2(110) at room temperature.[5] However, our recent TPD[6] and STM[7,8] works reveal that O_2 oxidation of reduced TiO_2(110) surfaces is much more complex than a simple vacancy filling process. At typical oxidation temperatures (500

* Corresponding author. E-mail: ma.henderson@pnl.gov.
† Present address: Goal line Environmental Technologies, 11141 Outlet Dr., Knoxville, TN 37932.

10.1021/jp990655q CCC: $18.00
Published on Web 06/06/1999

to 800 K), crystals with moderate-to-high bulk Ti interstitial defect densities exhibit a diverse variety of surface restructurings that include formation of hexagonal rosettes, strands, and (1 × 1) islands.[8] These surface structures result from oxidation of Ti interstitials that diffuse from the bulk to the surface. (The opposite effect occurs during vacuum annealing.[9]) At lower oxidation temperatures (300−500 K), molecular oxygen dissociatively fills vacancies, but does not draw Ti from the bulk of the crystal. Under these conditions, vacancies are filled in a 1:1 ratio with molecular oxygen with oxygen atom filling the vacancy and the remaining oxygen atom being deposited at a five-coordinate Ti^{4+} site as an adatom. These adatoms have been shown to significantly perturb the surface chemistry of co-adsorbed water,[6] ammonia,[6] and methanol[10] by facilitating O−H/N−H bond cleavage.

This study, however, focuses on the relatively unexplored aspect of O_2 chemistry seen only at very low temperatures (<200 K), that of molecular adsorption. Molecularly adsorbed O_2 species have been detected by the Yates group[11−14] using photodesorption after 100 K O_2 adsorption on TiO_2(110) with surface vacancy sites present. They observed unusual temperature dependences in the O_2 photodesorption and CO photooxidation yields that suggested adsorbed O_2 undergoes structural and/or site rearrangements during heating. Although they did not spectroscopically identify these species, their studies with mixed isotopes of oxygen indicated that O_2 was molecularly adsorbed. This conclusion is similar to results obtained by Beck et al.[15] and by Yanagisawa and Ota[16] for O_2 adsorption below 150 K on powdered TiO_2 rutile. In particular, these authors observed oxygen desorption states below 200 K and above 400 K that they attributed to desorption of molecularly bound O_2. Results in this study will show that O_2 adsorbs molecularly at vacancy sites if the adsorption temperature is below 150 K, desorbing at 410 K in TPD with a binding energy of 108 kJ/mol. At saturation, each vacancy is responsible for the adsorption of three molecules, presumably due to delocalization of the defect's band gap electron density to adjacent cation sites. Molecules bound at the vacancies dissociatively fill these sites during heating, whereas molecules bound at adjacent five-coordinate cation sites desorb at 410 K. Dissociative adsorption, however, is the dominant channel for adsorption temperatures above 150 K.

2. Experimental Section

The experiments in this study were performed in two separate ultrahigh vacuum (UHV) systems,[17,18] using two different TiO_2(110) crystals (Marketech International and Princeton Scientific). The as-received crystals were mounted in a manner described previously,[18] cleaned by sputtering with Ar^+ ions and annealing at 850 K. Both crystals were blue in color and were transparent. After the sputter/anneal treatments, no contaminants were detected by Auger electron spectroscopy (AES). Furthermore, a sharp (1 × 1) low-energy electron diffraction (LEED) pattern was observed from both crystals. TPD spectra from both chambers were performed with a 2 K/s ramp. The data obtained using these different systems and crystals were in complete agreement. The experimental procedure used to obtain the TPD spectra consisted of annealing the crystal at 850 K for 10 min in UHV, to induce the formation of surface oxygen vacancies, and subsequent exposure of the crystal at the desired temperature to research-grade purity gases. Each TPD experiment, unless otherwise specified, was performed on a freshly annealed surface. The manifold gas lines were conditioned to the gases by prolonged exposure prior to use. ELS measurements were performed in the specular scattering geometry with a primary electron beam energy of 20−25 eV. All spectra were recorded at 120 K.

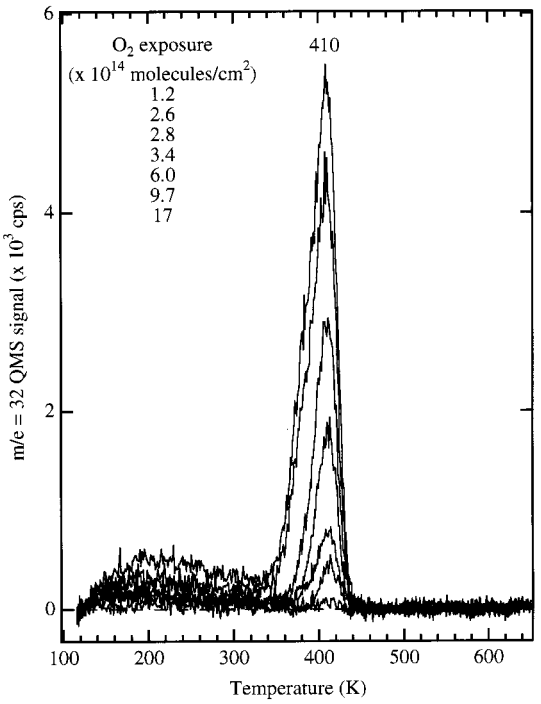

Figure 1. TPD spectra of O_2 (m/e = 32) adsorbed on the vacuum-annealed TiO_2(110) surface at 120 K. Exposures were performed through the directional doser.

O_2 was exposed to the vacuum-annealed TiO_2(110) surface by two methods, directional dosing and chamber backfilling. These two exposure methods gave essentially the same O_2 TPD behavior. Directional dosing results in minimal exposure of O_2 to surfaces other than that of the crystal, and thus yields O_2 TPD spectra with minimal interference from background desorption signals. However, saturation O_2 coverages could not be reached using the directional doser without long exposure times (in which background adsorption effects are a risk) or large O_2 gasline pressures (which exceed the effusive limits of the pinhole doser). Saturation coverages are more easily obtained by backfilling the chamber. However, artifacts in TPD from adsorption on extraneous surfaces were more prominent with backfilling, as will be shown.

The surface vacancy population was calibrated using H_2O TPD, as discussed in previous works.[20,21] Annealing the crystal at 850 K for 10 min typically resulted in an oxygen vacancy population of about 8% (or about 4×10^{13} sites/cm^2) of the bridging oxygen atoms on the ideal TiO_2(110) surface. This value is consistent with results obtained by STM under similar annealing conditions. The term "vacuum-annealed TiO_2(110)" is used throughout this paper to refer to a TiO_2(110) surface with 8% oxygen vacancy sites reproducibly obtained by annealing in UHV at 850 K for 10 min.

3. Results and Discussion

3.1. O_2 Adsorption at 120 K. Figures 1 and 2 shows O_2 TPD spectra (m/e = 32) from various O_2 exposures dosed at 120 K on the vacuum-annealed TiO_2(110) surface using the directional dosing method (a cartoon of the dosing configuration is shown in the inset of Figure 3). No O_2 features are observed in TPD for exposures below about 1.2×10^{14} molecules/cm^2. Exposures above this value yield a single TPD feature at about

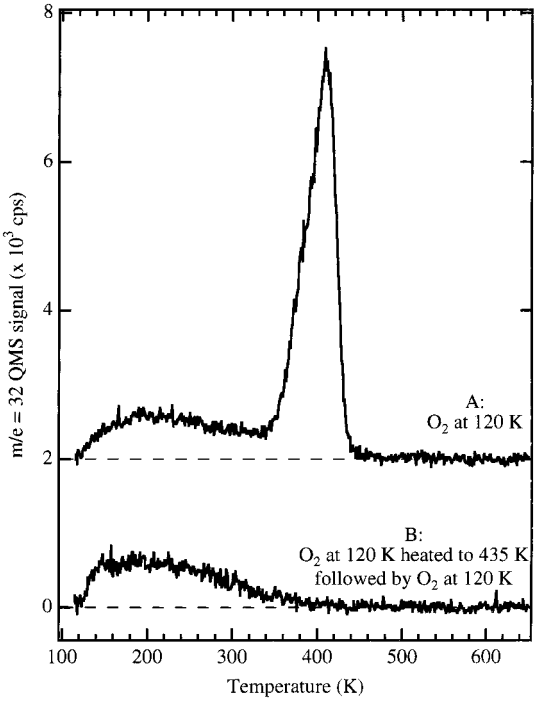

Figure 2. TPD spectra of O_2 ($m/e = 32$) following readsorption of O_2 on a previously heated O_2 adlayer on the vacuum-annealed $TiO_2(110)$ surface. Spectrum A corresponds to a 1.7×10^{15} molecules/cm^2 O_2 exposure at 120 K (same as in Figure 1), and spectrum B corresponds to a 1.3×10^{15} molecules/cm^2 O_2 exposure on a previous 1.3×10^{15} molecules/cm^2 O_2 exposure that was first heated through the TPD peak to 435 K. All exposures were at 120 K using the directional doser.

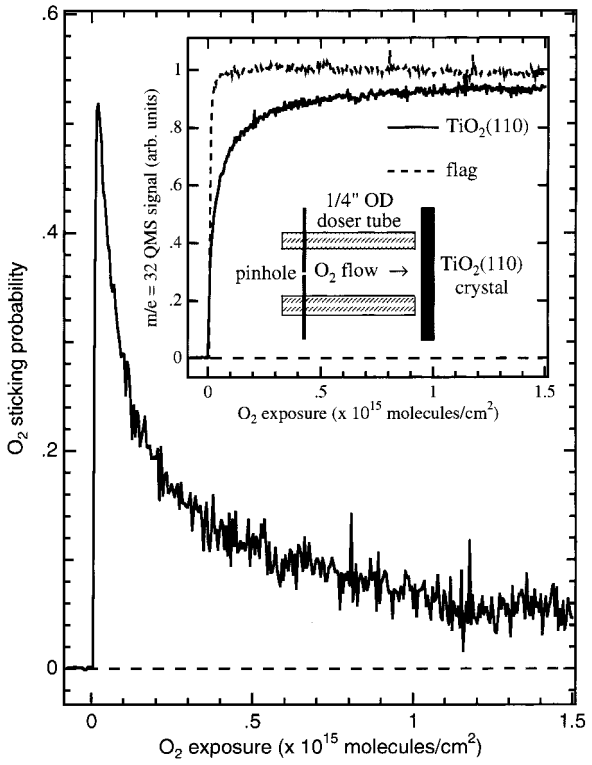

Figure 3. King and Wells uptake of O_2 on the vacuum-annealed $TiO_2(110)$ surface at 120 K. The inset shows the QMS response at $m/e = 32$ for O_2 striking the $TiO_2(110)$ crystal (at 120 K, solid line) and a stainless steel flag (at 300 K, dashed line). The main portion of the figure shows the difference of these two traces.

410 K that grows in intensity with increasing O_2 exposure. The absence of coverage dependence in this peak's desorption temperature is suggestive of first-order kinetics. The series of O_2 TPD spectra for exposures up to 9×10^{14} molecules/cm^2 can be adequately fit to first-order desorption kinetics without coverage dependence in the activation energy or preexponential, yielding values of 108 kJ/mol and of 1×10^{13} s^{-1}, respectively (the preexponential value was not assumed, but was obtained from the fitting process). Two additional features appear in the TPD at higher O_2 exposures. The first is a low-temperature shoulder on the 410 K TPD peak appearing for O_2 exposures above about 9×10^{14} molecules/cm^2. This feature is more apparent in TPD spectra from very high O_2 exposures obtained by backfilling the chamber (see below). The second feature is located between 120 and 400 K and is due to O_2 desorption from the sample holder.

The vacuum-annealed $TiO_2(110)$ surface is altered by each O_2 TPD experiment in that the vacancy sites are oxidized. Data in Figure 2 indicate that O_2 adsorption sites responsible for binding O_2 molecules in the 410 K TPD peak are not available after TPD unless the surface is reannealing at 850 K in UHV. Figure 2A shows the O_2 TPD spectrum ($m/e = 32$) from a 1.7×10^{15} molecules/cm^2 exposure dosed (through the doser) at 120 K (data from Figure 1). A similar O_2 exposure (1.3×10^{15} molecules/cm^2) was heated to 435 K and recooled to 120 K for another O_2 exposure before TPD (Figure 2B). This spectrum indicates that the 410 K O_2 TPD peak is not present for the second O_2 exposure. Comparison of the two O_2 TPD traces in Figure 2 reveals that O_2 adsorption sites are no longer available for subsequent O_2 adsorption after O_2 desorption. ELS data, to be discussed, indicate that the vacancies are oxidized during TPD of the first O_2 exposure. The O_2 TPD feature at 410 K is also not observed on a fully oxidized surface. Note, however, that the broad background between 120 and 400 K is still present in the second TPD spectrum (Figure 2B) indicating that it is probably not associated with the $TiO_2(110)$ surface.

The sticking probability and uptake of O_2 can be estimated using the King and Wells (KW) approach.[22] The KW data (Figure 3) were obtained using the directional dosing configuration shown in the inset. The 1/4 in. OD doser tube was positioned about 1 mm from the $TiO_2(110)$ crystal. A background O_2 signal was registered at the QMS (situated non-line-of-sight to the crystal face) before a valve was opened that isolated a gas line with 0.26 Torr O_2 from the pinhole. On opening the valve, an O_2 flux of 8.0×10^{12} molecules/(cm^2 s) impinged on the vacuum-annealed $TiO_2(110)$ surface at 120 K, with a coincident rise in the chamber O_2 partial pressure (solid line in the inset of Figure 3). The rise in the O_2 QMS signal was smaller when the O_2 stream impinged on the crystal (solid line in the inset of Figure 3) as compared to the signal from a stainless steel flag which resembles a square wave (dashed line). The difference between these two signals represents the sticking probability of O_2 on the vacuum-annealed $TiO_2(110)$ surface as a function of O_2 exposure. The initial sticking probability is high (greater than 0.5) but drops to below 0.2 within the first 1.5×10^{14} molecules/cm^2. The O_2 sticking probability continues to decrease with increasing exposure but maintains a value greater than about 0.05 up to an exposure of at least 1.5×10^{15} molecules/cm^2. The high initial sticking probability suggests that O_2 adsorption at 120 K is precursor-mediated. In contrast, Langmuirian adsorption into the oxygen vacancy sites would give an initial sticking probability no greater than about 0.08 resulting from the impact probability between the gaseous O_2 molecule and the vacancy.

Based on the determination of a nonunity sticking probability for O_2 on the vacuum-annealed $TiO_2(110)$ surface at 120 K,

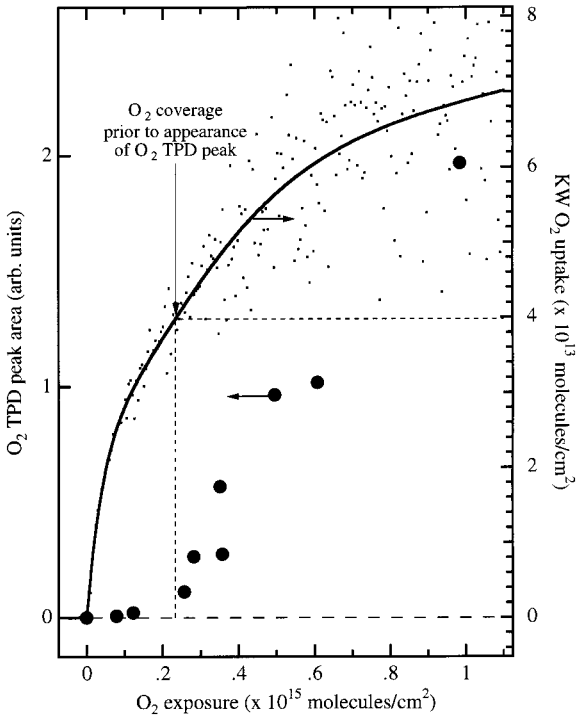

Figure 4. Comparison of the O_2 TPD peak areas from Figure 1 (circles; left-hand *y*-axis) with the raw (dots) and fitted (solid trace) King and Wells uptake data (right-hand *y* axis) obtained from Figure 2, all as a function of O_2 exposure at 120 K.

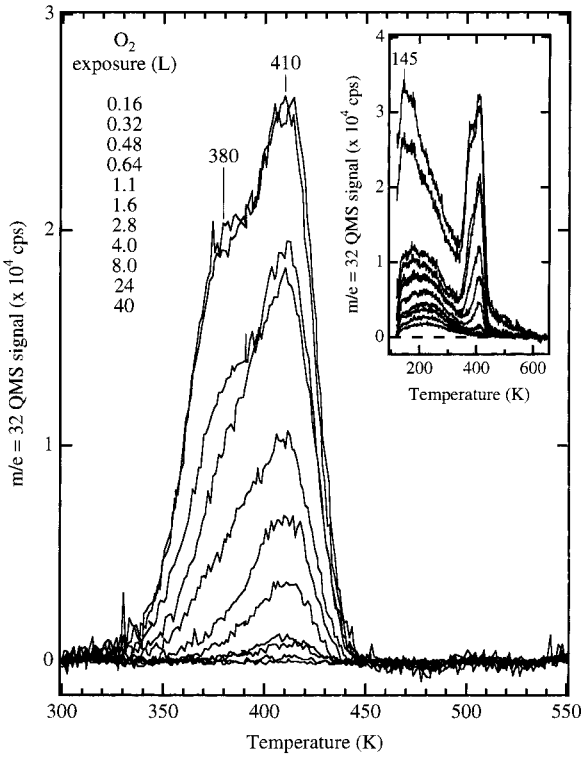

Figure 5. TPD spectra of O_2 ($m/e = 32$) on the vacuum-annealed TiO_2(110) surface at 120 K. Exposures were performed by backfilling. The inset shows the TPD spectra before subtraction of an exponential background from each trace.

problems may exist with the experimental setup shown in the inset of Figure 3 since many O_2 molecules may scatter from the crystal back into the doser tube eventually to be re-exposed to the crystal. Ideally, the KW method is performed with molecular beam dosing and sufficiently high chamber pumping speed so that re-exposure of scattered molecules is negligible. However, in this case, the doser does not provide a molecular beam and the chamber may not adequately pump scattered O_2 molecules in the 1 mm gap. Therefore, the actual O_2 exposures using the directional dosing method are probably slightly higher than those estimated by the O_2 conductance through the pinhole. Since this same problem exists for both the crystal and the stainless steel flag (which provided the square-wave background signal), the initial sticking probability of O_2 on the vacuum-annealed TiO_2(110) surface at 120 K is probably accurately measured. The exposures, however, cannot be corrected reliably. Note that the same dosing methodology was used for the data shown in Figure 1 enabling direct comparisons between the data in Figures 1 and 3 without errors in relative O_2 exposure.

The O_2 coverage on the vacuum-annealed TiO_2(110) surface at 120 K as a function of O_2 exposure is estimated by multiplying the exposure times the sticking probability (the *x* and *y* axes in Figure 3). This is displayed in Figure 4 as the KW uptake on the right axis, along with the TPD peak area from the 410 K O_2 state (large dots) plotted on the left axis. The solid line is a curve-fit through the KW uptake data points (small dots). As discussed above, there is virtually no O_2 desorption in TPD for exposures below about 2×10^{14} molecules/cm^2. The TPD peak area data in Figure 4 can be extrapolated to zero at an exposure of about 2.3×10^{14} molecules/cm^2. Examination of the KW uptake curve at this exposure reveals that the surface has adsorbed about 4×10^{13} molecules/cm^2 of O_2. This coverage of O_2 is approximately equal to the surface oxygen vacancy population (about 8% for this crystal after annealing at 850 K) estimated using H_2O TPD.[6] This *suggests* that the first 4×10^{13} molecules/cm^2 of adsorbed O_2 irreversibly fills the vacancies and that subsequently adsorbed O_2 molecules that evolve in TPD at 410 K are bound at sites *other than vacancies*. This conclusion does not imply that vacancy sites are not somehow associated with binding O_2 in the 410 K TPD state (especially since this state is only observed when the surface initially has vacancies) but that additional adsorption sites must exist on the surface because of the presence of the vacancies. This supposition is discussed in greater detail below.

Although the saturation coverage of O_2 at 120 K can conceivably be determined from the data in Figure 4 at higher exposures, errors resulting from the doser-crystal configuration preclude an accurate determination. Also, the scatter in the KW coverage estimate shown in Figure 4 for exposures above 3×10^{14} molecules/cm^2 greatly decreases the confidence of the least-squares fit of the data. Nevertheless, the KW data shown in Figure 4 suggests that about twice as much O_2 is adsorbed at an exposure of 1.1×10^{15} molecules/cm^2 as are vacancies present on the surface. This exposure is equivalent to a backfilling exposure of about 3.2 langmuirs (L). TPD data in Figure 5 from O_2 backfill exposures indicate the O_2 TPD uptake is only half saturated after an exposure of about 3 L. These data, taken together, indicate that the saturation O_2 uptake at 120 K is about 3 times the oxygen vacancy population, with two-thirds of the uptake recovered in TPD and one-third unrecovered.

Figure 5 shows O_2 TPD spectra ($m/e = 32$) obtained using the backfilling exposure method. The inset of Figure 5 shows the raw O_2 TPD data. Backfilling clearly enhances the amount of O_2 registered between 120 and 400 K. The chamber recovery time after each exposure varied, partially because different O_2 pressures were used. Pumping tails resulting from using large pressures are especially evident in the 24 and 40 L spectra. Nevertheless, these pumping tails were removed from the raw

data by subtraction of an exponential background, yielding the TPD traces shown in the main portion of Figure 5. Little or no O_2 desorption is observed for O_2 exposures below about 1 L. The 410 K O_2 TPD feature is prominent for exposures above 1 L, and a 380 K temperature shoulder is resolved for exposures above 8 L. The presence of this shoulder in TPD, however, is intermittent. Several O_2 TPD exposure series were conducted over the course of a year on two separate $TiO_2(110)$ crystals. The 380 K TPD shoulder was present in some of these TPD series and not in others. The presence or absence of this shoulder does not correlate with factors such as crystal "age" or water coadsorption. It is possible that this feature may be linked to some undetected bulk impurity or coadsorbed background gas. In addition to the 380 and 410 K TPD states, a third O_2 TPD peak is present at 145 K after very large exposures (see inset of Figure 5). This feature could be from a weakly bound form of O_2, possibly located at nondefect sites, or it could also be from background effects.

The TPD uptake plot using the backfilling method (not shown here) is similar to the plot shown in Figure 4 using the directional dosing method. The extrapolated exposure onset for O_2 desorption in the 410 K TPD peak is at about 0.88 L. A 0.88 L O_2 exposure corresponds to about an exposure in molecules/cm^2 of 3.2×10^{14}. This value is close to the 2.3×10^{14} molecules/cm^2 value obtained from directional dosing. The discrepancy between these two values lies either in the O_2 flux of the directional dosing method or the O_2 partial pressure during backfilling measured by the ion gauge.

3.2. Mixed $^{16}O_2/^{18}O_2$ Isotope Studies. Although the appearance of the 410 O_2 TPD state is suggestive of molecular desorption (as opposed to recombinative desorption), mixed oxygen isotope studies were conducted to test for dissociation. Exposure of a 1:1 mixture of $^{16}O_2 + {}^{18}O_2$ to the vacuum-annealed $TiO_2(110)$ surface at 120 K did not result in significant amounts of $^{16}O^{18}O$ in TPD above that expected for scrambling in the QMS ionizer. This, in itself, does not rule out O_2 dissociative adsorption since recombination could preferentially occur between the original pair of O atoms. However, spectroscopic evidence presented below, along with the first-order desorption behavior in TPD discussed above, supports the molecular desorption assignment.

Mixed isotope studies were also performed in order to explore the fate of adsorbed O_2 at 120 K prior to the exposure for the onset of the 410 K O_2 TPD feature. In these experiments, varying $^{18}O_2$ exposures on the vacuum-annealed $TiO_2(110)$ surface at 120 K are followed by 20 L of $^{16}O_2$, also at 120 K. The $^{18}O_2$ TPD spectra ($m/e = 36$) from these combinations of $^{16}O_2$ and $^{18}O_2$ are shown in Figure 6. (The accompanying $^{16}O_2$ TPD spectra ($m/e = 32$) are not shown for simplicity.) For comparison, the $^{18}O_2$ TPD data without postexposure of $^{16}O_2$ are also shown in Figure 6 (as filled spectra). In each case, more $^{18}O_2$ desorbs from the surface *after* postexposure of $^{16}O_2$ than without postexposure of $^{16}O_2$. This is especially evident for low $^{18}O_2$ exposures ($\leq$0.8 L) where little or no $^{18}O_2$ is recovered in TPD without postsaturation by $^{16}O_2$. These data suggest that O_2 does not dissociate upon adsorption at 120 K despite the absence of O_2 in TPD for exposures below 0.8 L. Instead, the data in Figure 6 suggests that at 120 K all adsorbed O_2 molecules, irrespective of the order in which they arrived at the surface, have an equal probability to desorb and an equal probability to decompose. For example, 0.8 L is approximately the backfilling exposure for the onset of O_2 desorption in the 410 K TPD state. This exposure gives a total $^{18}O_2$ coverage of about 4×10^{13} molecules/cm^2 based on comparison with the

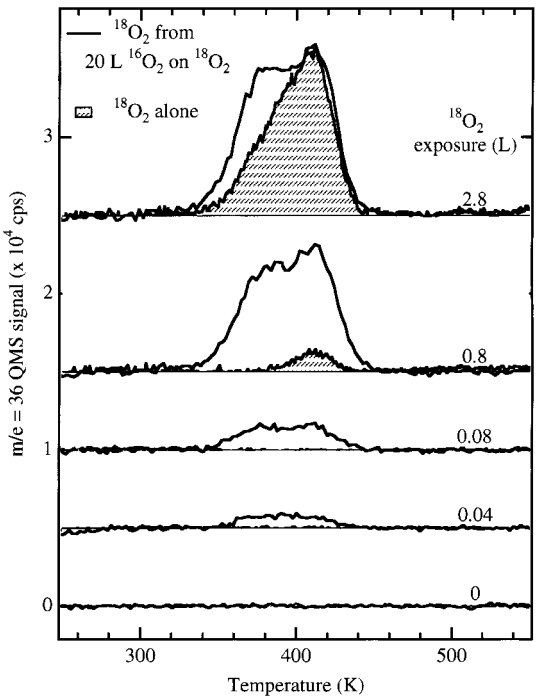

Figure 6. TPD spectra of $^{18}O_2$ ($m/e = 36$) from various backfilling exposures of $^{18}O_2$ adsorbed on the vacuum-annealed $TiO_2(110)$ surface at 120 K with (solid lines) and without (shaded lines) postexposure to 20 L of $^{16}O_2$ at 120 K. The corresponding $m/e = 32$ and 34 spectra are not shown for clarity; see text for description of those data.

directional dosing uptake results shown in Figure 4. If this coverage of $^{18}O_2$ were irreversibly bound and the remaining surface sites were saturated with $^{16}O_2$, then one would expect only $^{16}O_2$ to evolve in TPD. However, as shown for the 0.8 L $^{18}O_2$ exposure in Figure 6, a considerable amount of $^{18}O_2$ is desorbed along with $^{16}O_2$ (not shown). The resulting $^{18}O_2$ to $^{16}O_2$ TPD peak area ratio for this experiment was 1:2.3. If the partitioning of $^{16}O_2$ and $^{18}O_2$ between molecular and irreversible adsorption states in this experiment is purely statistical, then these data also suggest that the saturation uptake of O_2 is equivalent to 3 times the vacancy population. This assumption is supported by the expected statistical ratios of desorbed $^{16}O_2$ and $^{18}O_2$ in the other combinations of Figure 6. Therefore, it appears that the surface binds 3 times as much O_2 as there are available vacancy sites, in agreement with the estimated saturation coverage from the KW uptake and TPD measurements discussed above.

The data in Figure 6 also suggest that one of two possible processes occurs during O_2 adsorption at 120 K. The first possibility is that adsorption proceeds through a precursor state in which all adsorbed O_2 molecules reside at 120 K irrespective of their arrival order to the surface. Upon heating, each O_2 molecule bound in this precursor state has equal opportunities relative to its neighbors to fall into a molecularly bound state leading to desorption or into a state leading to dissociation. The second possibility is that initial adsorption does occur in a specific order (e.g., vacancy sites fill first and nonvacancy sites fill last), but that the barrier to O_2 (not O atom) exchange between these sites is lower than the barrier to O_2 dissociation at the vacancy sites. The former seems more plausible since data in Figure 3 indicate O_2 adsorption occurs through a precursor-mediated process. Interchange between sites cannot be ruled out however.

3.3. Coadsorption of O_2 and CO_2. Further insight into the adsorption of O_2 on the vacuum-annealed $TiO_2(110)$ surface is

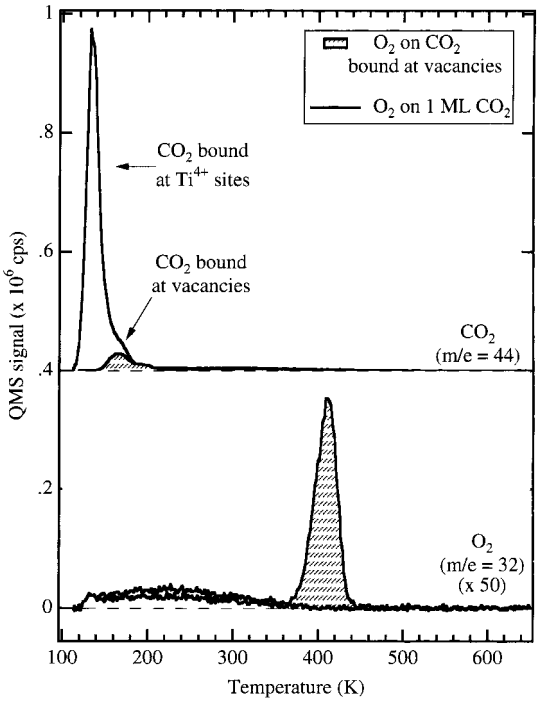

Figure 7. TPD spectra ($m/e = 32$ and 44) from coadsorption of O_2 and CO_2 on the vacuum-annealed TiO_2(110) surface at 120 K. Shaded traces in both O_2 and CO_2 TPD spectra correspond to spectra from an exposure of 1.9×10^{15} molecules/cm^2 O_2 to a surface with the vacancies filled with CO_2 (prepared by preheating a saturated CO_2 monolayer to 145 K). Solid (unfilled) traces correspond to spectra from an exposure of 1.9×10^{15} molecules/cm^2 O_2 exposed to a saturated CO_2 monolayer (one CO_2 for every exposed cation site). All exposures were performed using the directional doser to minimize background effects.

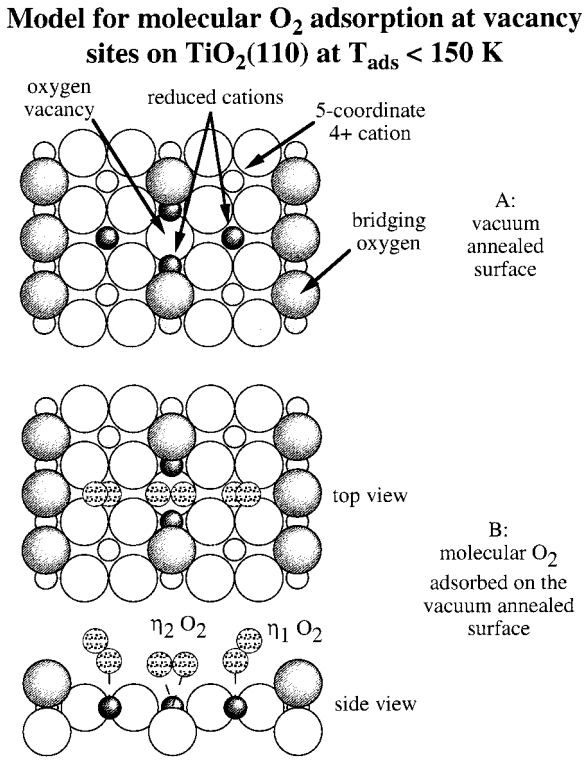

Figure 8. Schematic model for the bonding of O_2 to the vacuum-annealed TiO_2(110) surface. Model A shows the top view of the TiO_2(110) surface with an oxygen vacancy site. Model B shows top and side (along the [001] direction) views of O_2 molecules bonding at vacancy and nonvacancy sites.

obtained by performing coadsorption studies with CO_2. CO_2 by itself adsorbs nondissociatively on the vacuum-annealed TiO_2(110) surface, first at vacancy sites and then at five-coordinate Ti^{4+} sites.[21] Vacancy-bound CO_2 desorbs in a small peak at about 165 K and nonvacancy-bound CO_2 desorbs in a sharp, intense feature at about 135 K (Figure 7). A surface with CO_2 adsorbed only in the vacancies can be prepared by preheating a saturation CO_2 coverage to 145 K. Exposure of this surface to O_2 at 120 K does not result in displacement of CO_2 from the vacancy sites (shaded $m/e = 44$ trace in Figure 7), but neither is O_2 adsorption into the 410 K TPD state blocked by the vacancy-bound CO_2 (shaded $m/e = 32$ trace in Figure 7). KW analysis of the O_2 uptake on a surface with the vacancies filled with CO_2 reveals a decrease in the initial O_2 sticking probability to about 0.4 and a decrease in the total O_2 uptake of at least 2×10^{13} molecules/cm^2 (data not shown). This deficiency is most likely in the irreversibly O_2 adsorbed channel, since the peak area in the 410 K O_2 TPD state of Figure 7 is only slightly less than that for a similar O_2 exposure on the CO_2-free surface (Figure 1). This suggests that after CO_2 desorbs from the vacancy sites at 165 K adsorbed O_2 molecules at nonvacancy sites do not move into the available vacancies and the vacancy sites are not oxidized. Note also that the data in Figure 7 indicate that a fully saturated CO_2 monolayer, which comprises one CO_2 molecule per exposed surface cation site, completely blocks *all* O_2 adsorption.

3.4. Proposed Model for Adsorbed O_2. Figure 8 shows a proposed model for O_2 on the vacuum-annealed TiO_2(110) surface based on the results in Figures 1−7. The model in Figure 8A shows an oxygen vacancy site on the clean TiO_2(110) surface. Recent STM images suggest that the majority of oxygen vacancy sites on the vacuum-annealed TiO_2(110) surface (after cooling to room temperature) are isolated vacancies.[7] It is commonly held in the literature that these isolated oxygen vacancy sites possess reduced Ti cations, probably in the 3+ oxidation state, based on numerous spectroscopic studies.[23] For example, UPS shows a state located in the band gap,[4] and ELS shows a loss process at about 0.8 eV[6,21,24,25] for the vacuum-annealed surface. Several theoretical studies predict that the electrons associated with oxygen vacancies on TiO_2(110) are localized on the Ti atoms directly at the vacancy sites.[26−28] The supposition of electron localization is generally held by experimentalists examining the electronic structure of defective TiO_2 surfaces.[23] Recently, however, two density functional theory (DFT) studies have included spin-polarization in calculating the electronic structure of oxygen vacancies on TiO_2(110). Lindan et al.[29] determined that the inclusion of occupancy of "... spin-unpaired orbitals rather than the partial occupancy of spin-paired orbitals reduces the on-site exchange energy but increases the kinetic energy". They further conclude that the exchange term dominates such that the overall energy of the surface is lowered by including spin-polarization, and the proper energy of the band gap state below the conduction band edge is predicted. Although these authors did not conclude that the unpaired electrons were delocalized to other surface sites, a second DFT calculation including spin-polarization performed by Paxton and Thien-Nga[30] found that electron density in spin-polarized states is partially delocalized to the adjacent five-coordinate Ti^{4+} cations (see Figure 8A). These authors also conclude that the total energy of the surface is lower with inclusion of spin-polarization. The two types of reduced cation sites depicted in Figure 8A may not be easily differentiated by STM due to nonspecific tunneling. However, a line scan along the [110] direction over a vacancy shows a fairly uniform tunneling distance in the constant current mode over all three sites (the vacancy and two five-coordinate Ti^{4+} sites).[7] One

might have expected instead that an oxygen vacancy would appear as a resolved spot, unconnected to the adjacent cation sites. Therefore, it seems likely that five-coordinate Ti^{4+} sites adjacent to an oxygen vacancy might instead be partially reduced, possessing sufficient electron density from the vacancy to facilitate charge-transfer stabilization of O_2. The model in Figure 8 therefore corresponds to three O_2 molecules sharing the two electrons associated with each vacancy site.

The absence of O_2 adsorption on the fully oxidized surface at 120 K suggests that a reduced cation site is required to form a strong adsorption bond between the surface and O_2. Since the KW uptake and TPD measurements suggest that the total amount of O_2 adsorbed on the vacuum-annealed $TiO_2(110)$ surface is about 3 times the vacancy population, the proposition by Paxton and Thien-Nga[30] that the vacancy electrons are delocalized may explain the behavior of O_2 on the vacuum-annealed $TiO_2(110)$ surface. Figure 8B shows top and side (along the [001] direction) views illustrating possible bonding configurations for O_2 at the three sites around a vacancy that Paxton and Thien-Nga have proposed to spin density. The purpose of this cartoon is not to stipulate the exact bonding of O_2, but to propose that it is spatially possible to fit O_2 molecules into each site without apparent steric hindrance. (For clarity, the lattice atoms are shown as ionic species and the O_2 molecules are shown as covalent species.) There are a variety of two-centered (bridging between two metal atoms) bonding configurations for O_2 known in the inorganic literature,[31] but the most obvious configuration given the steric constraints of the vacancy site is the η^2 complex ("η^n", in the inorganic nomenclature, refers to a ligand employing n atoms in bonding[31]). Single metal-centered bonding configurations of O_2 can be either η^1 or η^2 complexes, but chemical intuition suggests that a nonvacancy-bound species at a five-coordinate Ti cation site is probably the former. In both cases, charge transfer from the cation to the O_2 molecule is needed for adsorption, so the O_2 molecules are probably charged slightly negative. The van der Waals radius of a covalent oxygen atom is about 1.4 Å.[32] Using an O−O bond distance of 1.3 Å, which is approximately that for most O_2^- complexes,[33] there is only a slight degree of overlap between the van der Waals radii of the vacancy-bound and nonvacancy-bound O_2 species shown in Figure 8B. We propose that the η^1 species in our model desorbs in the 410 K O_2 TPD peak and the η^2 species decomposes to an oxygen adatom and a filled vacancy site. This latter process is discussed in more detail below.

3.5. Electron Spectroscopic Evidence for Adsorbed O_2^-. In an effort to identify the O_2 species responsible for the 410 K O_2 TPD peak, vibrational (HREELS) and electronic (ELS) spectroscopy were attempted. HREELS of the vacuum-annealed surface after saturation with O_2 at 120 K did not show distinct losses due to adsorbed O_2, but did show additional loss intensity in the region between the high-loss energy tail of the intense 755 cm^{-1} primary phonon loss and the less intense 1190 cm^{-1} phonon remnant (see ref 34 for phonon spectrum of $TiO_2(110)$). Intensity in this spectral region is consistent with the ν(O−O) stretch of O_2^- complexes, whereas the ν(O−O) stretches of O═O and O−O species appear at higher and lower frequencies, respectively.[33]

ELS measurements, shown in Figure 9, yielded the stronger spectroscopic evidence for an adsorbed O_2^-. Figure 9a shows the ELS spectrum for the vacuum-annealed $TiO_2(110)$ surface. As in previously published spectra,[6,21,24,25] the vacuum-annealed $TiO_2(110)$ surface gives an intense loss feature at about 0.8 eV corresponding to polaron excitation of the electrons at the

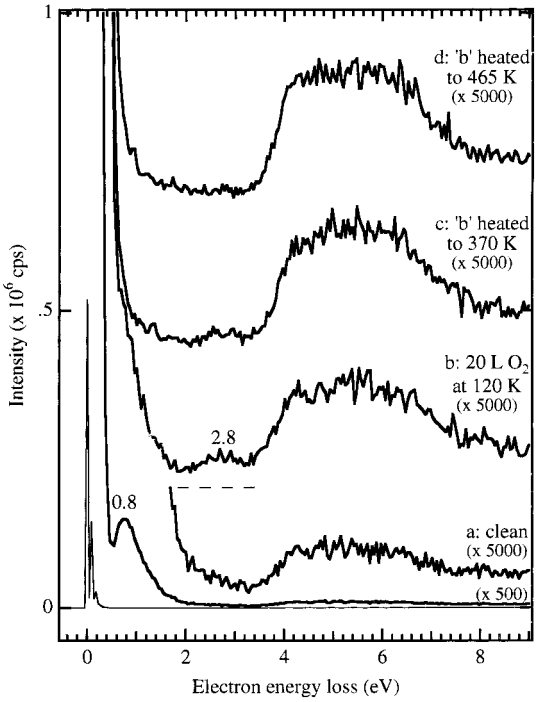

Figure 9. ELS spectra from the clean vacuum-annealed $TiO_2(110)$ surface (a) and after exposure to 20 L O_2 at 120 K (b) followed by heating to 370 (c) and 465 K (d). The electron energy is 25 eV.

vacancy sites. The band-to-band transitions are located above 3 eV. Exposure of the vacuum-annealed $TiO_2(110)$ surface to 20 L O_2 at 120 K results in a new loss feature at 2.8 eV and a significant decrease in the 0.8 eV loss feature (Figure 9b). The 2.8 eV loss persists in the ELS spectrum after heating to 370 K (Figure 9c) but is absent after heating to 465 K (Figure 9d). This suggests that the 2.8 eV loss is associated with the desorption of molecular O_2 at 410 K. This loss energy (which would be at about 440 nm in the optical spectrum) is consistent with the electronic spectra of inorganic Ti−O_2^- complexes. For example, Jeske et al.[35] observed optical absorption features at 410−430 nm in UV−vis as the result of complexing O_2 with various Ti^{3+} complexes, which along with X-ray crystallography and IR, lead to an assignment of an η^2 O_2^- bound ligand. In published work on $TiO_2(110)$, Göpel et al.,[36] using conductivity and work function change measurements, also proposed that an O_2^- species forms from the interaction of molecular oxygen with vacancies.

Note that the ELS spectrum in Figure 9d is featureless below 3 eV after heating to 465 K, despite the fact that our previous work[6] indicates oxygen adatoms are present on the surface. The absence of loss features from these oxygen adatoms is consistent with UV−vis spectra of Ti═O complexes that are transparent at wavelengths above about 300 nm (below about 4 eV).[35]

3.6. Dependence of O_2 Adsorption Temperature. On the basis of data in the previous sections, there appear to be two main thermal channels for O_2 adsorbed on the vacuum-annealed $TiO_2(110)$ surface at 120 K: molecular desorption at 410 K and irreversible decomposition with O atom vacancy filling. However, only the irreversible channel is followed at higher adsorption temperatures, as will be shown below.

Figure 10 shows O_2 TPD spectra ($m/e = 32$) after adsorption of 40 L O_2 at various temperatures on the vacuum-annealed $TiO_2(110)$ surface. The 410 K TPD peak is intense at an adsorption temperature of 100 K but decreases dramatically as the adsorption temperature is raised to 160 K. No O_2 TPD signal is detected for adsorption temperatures at or above 180 K. The

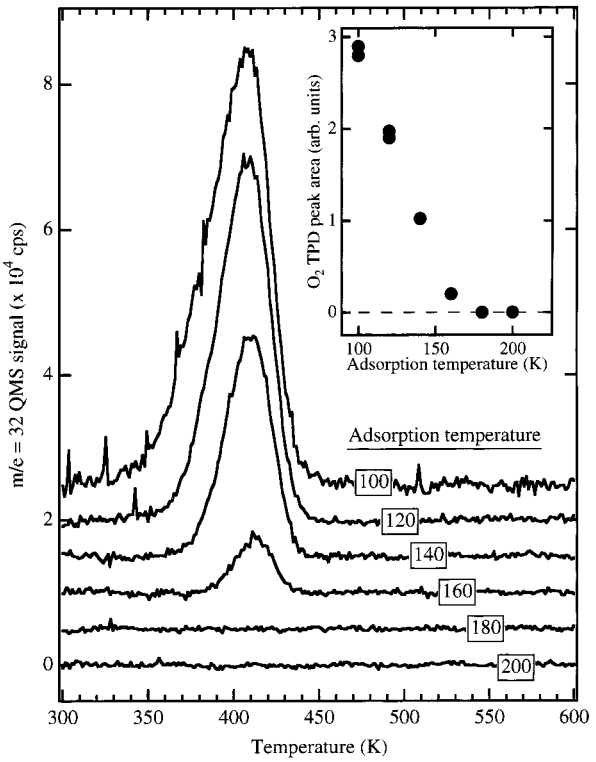

Figure 10. Adsorption temperature dependence in the O_2 TPD ($m/e = 32$) for a 40 L exposure on the vacuum-annealed TiO_2(110) surface. Backgrounds are removed from the data in the same manner as for the data in Figure 4. The inset shows the O_2 TPD peak area in the 410 K state as a function of adsorption temperature.

inset to Figure 10 shows that the O_2 TPD area decreases linearly with adsorption temperature between 100 and 160 K. The initial O_2 sticking probability decreases by at least 50% at 200 K (as compared to 120 K), as indicated by KW uptake measurements (data not shown). However, the surface still adsorbs O_2 at the higher adsorption temperatures, although irreversibly (i.e., without O_2 in TPD at 410 K). This is demonstrated by the ELS measurements shown in Figure 11. Adsorption of O_2 at 120 (solid traces) and 300 K (dashed traces) both oxidize the vacancies, as evidenced by removal of the loss at 0.8 eV observed on the vacuum-annealed surface (dotted trace). However, O_2 adsorption at 300 K does not result in the 2.8 eV loss feature attributed to the molecular O_2 species that desorbs at 410 K in TPD. Therefore, the decrease in the 410 K O_2 TPD peak area with increasing adsorption temperature (inset of Figure 10) is linked to oxidation of the vacancy sites and removal of electron density necessary for charge transfer formation of the O_2^- species.

Data in Figure 12 further illustrate the competition between the molecular and dissociative oxygen channels on the vacuum-annealed TiO_2(110) surface. The solid trace is the TPD spectrum from a 2.4 L exposure of $^{18}O_2$ on the vacuum-annealed TiO_2(110) surface at 120 K. This exposure corresponds to a surface $^{18}O_2$ coverage of about half saturation of all available molecular oxygen adsorption sites. The shaded trace of Figure 12 is also the TPD spectrum for a total 2.4 L $^{18}O_2$ exposure, except that this was done in two steps. The first step involved a 0.8 L exposure at 120 K, followed by heating the crystal to 200 K, recooling to 120 K, and then the second step involving exposure of 1.6 L (to give a total of 2.4). The initial 0.8 L exposure corresponds to an O_2 coverage that is approximately equivalent to the vacancy coverage (see above). Comparison of the two TPD traces in Figure 12 reveals that the adsorption

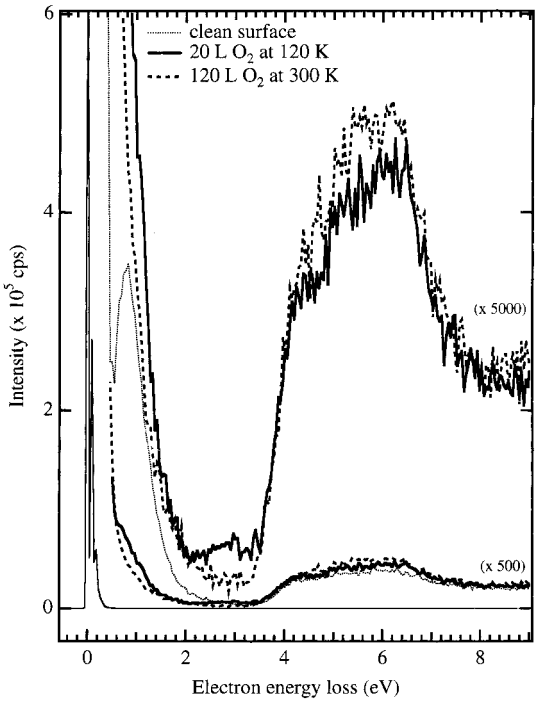

Figure 11. ELS spectra for the vacuum-annealed TiO_2(110) surface (dotted trace), and for saturation O_2 exposed to the vacuum-annealed TiO_2(110) surface at 120 K (solid traces) and 300 K (dashed traces). The electron energy was 25 eV.

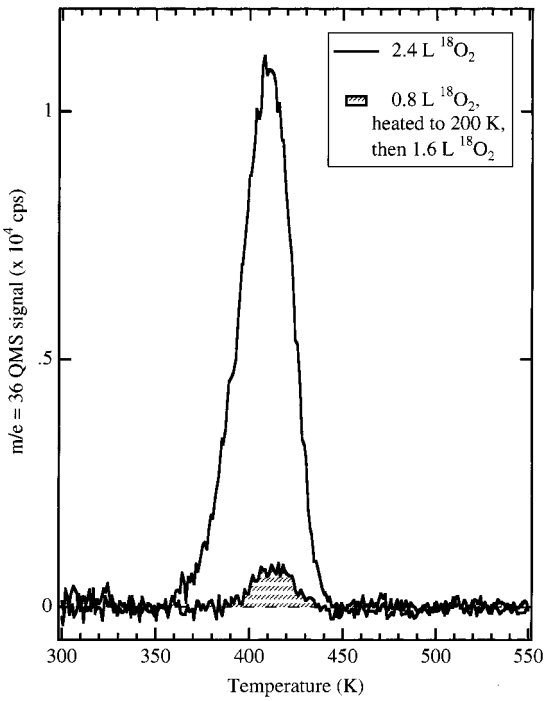

Figure 12. TPD spectra of $^{18}O_2$ ($m/e = 36$) from a total 2.4 L exposure on the vacuum-annealed TiO_2(110) surface performed in one step (solid trace) and in two steps, 0.8 L + 1.6 L (shaded trace), with preheating of the surface to 200 K between the two steps. All exposures are by backfilling at 120 K.

sites for molecular $^{18}O_2$ in the 1.6 L exposure are blocked by preheating the 0.8 L exposure up to 200 K. The $^{18}O_2$ TPD peak in the shaded trace is only slightly less (in peak area) than what is observed for a 0.8 L exposure by itself (see Figure 5). The essence of the results in Figure 12 can also be realized by using a mixture of O_2 isotopes. If the second exposure in the two-step process of Figure 12 is with a different oxygen isotope,

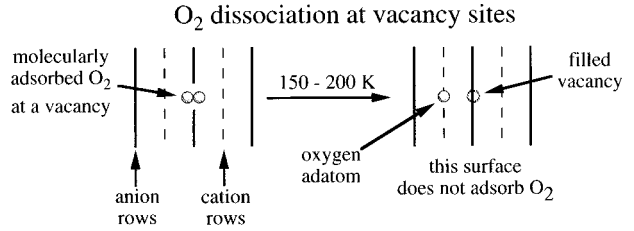

Figure 13. Schematic models for the temperature dependence in the molecular and dissociative channels of O_2 on the vacuum-annealed TiO_2(110) surface. See text for description of the models.

only the oxygen isotope in the first exposure is observed in TPD (data not shown).

Figure 13 presents a schematic model for the dissociative filling of vacancy sites by O_2 adsorption on the vacuum-annealed TiO_2(110) surface. At low adsorption temperatures (<150 K), O_2 molecules adsorb through a precursor-mediated process. At some temperature between the adsorption temperature and 200 K, the ensemble of O_2 molecules is partitioned between the molecular adsorption sites and the dissociative adsorption sites (vacancies). At low coverage, were no molecular desorption is detected, the vacancy-bound O_2 molecules dissociatively fill the vacancies before 200 K, leaving an oxygen adatom on the surface. (The chemistry of this oxygen adatom is the focus of a previous paper.[6]) Once the vacancy sites are filled, the surrounding cation sites are no longer active for O_2 adsorption, even after recooling to 120 K. The case at higher O_2 coverages is less clear because the data in Figure 12 suggest that both molecular and dissociative species coexist on the surface as the temperature is raised to 200 K. The dissociative filling of vacancies does not seem to affect preadsorbed O_2 molecules in the molecular channel, but prevents additional O_2 molecules from being adsorbed. At present, there is no clear understanding for this since dissociation at the vacancy should remove electron density from the O_2^- species at the five-coordinate Ti cation sites resulting in a destabilized Ti−O_2 bond and desorption. Although this model is speculative, it provides a framework for better understanding the chemistry of O_2 on TiO_2.

There are two ways to interpret the shift toward dissociative O_2 chemistry with increasing adsorption temperature. The first, and perhaps most obvious, interpretation is in terms of more favorable kinetics for O_2 dissociation with increasing adsorption temperature. This possibility would imply that O_2 dissociation is an activated process. The second interpretation is that the electron density and/or spin state of the electrons in the vicinity of the vacancy dictates molecular versus dissociative adsorption and that a temperature-dependent redistribution (such as a spin-polarized to spin-unpolarized transition) of the vacancy electrons occurs at about 150−200 K. As it were, this temperature range is consistent with the antiferromagnetic to nonmagnetic transition for the Magneli phases of TiO_2 rutile,[37−39] although no such transition has been observed with slightly reduced TiO_2. Unfortunately, no information exists in the literature for the temperature-dependent spin transitions at isolated vacancy sites.

Conclusions

The low-temperature chemistry of O_2 at vacancy sites on the TiO_2(110) surface is surprisingly rich and complex. At adsorption temperatures below 150 K, oxygen adsorbs with a high initial sticking probability suggestive of precursor-mediated kinetics. Evidence is found for both molecular and dissociative channels, with strong adsorption temperature dependence between these two channels. The dissociative channel is favored above an adsorption temperature of 150 K. However, molecularly adsorbed species formed by adsorption below 150 K are stable on the surface until 410 K. ELS results suggest that these molecularly adsorbed O_2 molecules are present on the surface as O_2^-. Formation of this O_2^- species requires oxygen vacancy sites, although the vacancies need not be directly involved in binding the O_2^- species. TPD and uptake measurements indicate that each surface oxygen vacancy site is responsible for binding up to three O_2 molecules, suggesting that the electron density associated with the vacancy is delocalized to adjacent cation sites.

Acknowledgment. This work was supported by the U.S. Department of Energy, Office of Basic Energy Sciences, Division of Materials Sciences, and the Environmental Management Science Program. Pacific Northwest National Laboratory is a multiprogram national laboratory operated for the U.S. Department of Energy by Battelle Memorial Institute under Contract DE-AC06-76RLO 1830. The research reported here was performed in the William R. Wiley Environmental Molecular Science Laboratory, a Department of Energy user facility funded by the Office of Biological and Environmental Research. Ulrike Diebold acknowledges partial support from an NSF-CAREER grant.

References and Notes

(1) Fox, M. A.; Dulay, M. T. *Chem. Rev.* **1993**, *93*, 341.
(2) Mills, A.; Davies, R. H.; Worsley, D. *Chem. Soc. Rev.* **1993**, *22*, 417.
(3) Linsebigler, A. L.; Lu, G.; Yates, J. T., Jr. *Chem. Rev.* **1995**, *95*, 735.
(4) Kurtz, R. L.; Stockbauer, R.; Madey, T. E.; Roman, E.; de Segovia, J. L. *Surf. Sci.* **1989**, *218*, 178.
(5) Pan, J. M.; Maschhoff, B. L.; Diebold, U.; Madey, T. E. *J. Vac. Sci. Technol., A* **1992**, *10*, 2470.
(6) Epling, W. S.; Peden, C. H. F.; Henderson, M. A.; Diebold, U. *Surf. Sci.* **1998**, *412/413*, 333.
(7) Diebold, U.; Lehman, J.; Mahmoud, T.; Kuhn, M.; Leonardelli, G.; Hebenstreit, W.; Schmid, M.; Varga, P. *Surf. Sci.* **1998**, *411*, 137.
(8) (a) Li, M.; Hebenstreit, W.; Diebold, U. *Surf. Sci.* **1998**, *414*, L951. (b) Li, M.; Hebenstreit, W.; Diebold, U.; Henderson, M. A.; Jennison, D. R.; Schultz, P. A.; Sears, M. P. *Surf. Sci.*, in press.
(9) Henderson, M. A. *Surf. Sci.* **1999**, *419*, 174.
(10) Henderson, M. A.; Otero-Tapia, S.; Castro, M. E. *Phys. Chem. Chem. Phys.*, submitted.
(11) Lu, G.; Linsebigler, A.; Yates, J. T., Jr. *J. Chem. Phys.* **1995**, *102*, 3005.
(12) Lu, G.; Linsebigler, A.; Yates, J. T., Jr. *J. Chem. Phys.* **1995**, *102*, 4657.
(13) Linsebigler, A.; Lu, G.; Yates, J. T., Jr. *J. Phys. Chem.* **1996**, *100*, 6631.
(14) Rusu, C. N.; Yates, J. T., Jr. *Langmuir* **1997**, *13*, 4311.
(15) Beck, D. D.; White, J. M.; Ratcliffe, C. T. *J. Phys. Chem.* **1986**, *90*, 3132.
(16) Yanagisawa, Y.; Ota, Y. *Surf. Sci.* **1991**, *254*, L433.
(17) Henderson, M. A. *Surf. Sci.* **1994**, *319*, 315.
(18) Herman, G. S.; Peden, C. H. F. *J. Vac. Sci. Technol. A* **1994**, *12*, 2087.
(19) Brinkley, D.; Dietrich, M.; Engel, T.; Farrall, P.; Gantner, G.; Schafer, A.; Szuchmacher, A. *Surf. Sci.* **1998**, *395*, 292.
(20) Henderson, M. A. *Langmuir* **1996**, *12*, 5093.
(21) Henderson, M. A. *Surf. Sci.* **1998**, *400*, 203.
(22) King, D. A.; Wells, M. G. *Surf. Sci.* **1972**, *29*, 454.
(23) Henrich, V. E.; Cox, P. A. *The Surface Science of Metal Oxides*; Cambridge University Press: Cambridge, 1994.
(24) Göpel, W.; Anderson, J. A.; Frankel, D.; Jaehnig, M.; Phillips, K.; Schaefer, J. A.; Rocker, G. *Surf. Sci.* **1984**, *139*, 333.
(25) Rocker, G.; Schaefer, J. A.; Göpel, W. *Phys. Rev. B* **1984**, *30*, 3704.
(26) Munnix, S.; Schmeits, M. *J. Vac. Sci. Technol., A* **1987**, *5*, 910.
(27) Chun-Ru, W.; Yin-Sheng, X. *Surf. Sci.* **1989**, *219*, L537.
(28) Kobayashi, H.; Yamaguchi, M. *Surf. Sci.* **1989**, *214*, 466.
(29) Lindan, P. J. D.; Harrison, N. M.; Gillan, M. J.; White, J. A. *Phys. Rev. B* **1997**, *55*, 15919.
(30) Paxton, A. T.; Thien-Nga, L. *Phys. Rev. B* **1998**, *57*, 1579.
(31) Cotton, F. A.; Wilkinson, G. *Advanced Inorganic Chemistry*, 5th ed.; John Wiley and Sons: New York, 1988.

(32) *Handbook of Chemistry and Physics*, 57th ed.; Weast, R. C., Ed.; CRC Press: Cleveland, OH, 1977.
(33) Vaska, L. *Acc. Chem. Res.* **1976**, *9*, 175.
(34) Henderson, M. A. *Surf. Sci.* **1996**, *355*, 151.
(35) Jeske, P.; Haselhorst, G.; Weyhermuller, T.; Wieghardt, K.; Nuber, B. *Inorg. Chem.* **1994**, *33*, 2462.
(36) Göpel, W.; Rocker, G.; Feierabend, R. *Phys. Rev. B* **1983**, *28*, 3427.
(37) Bartholomew, R. F.; Frankl, D. R. *Phys. Rev.* **1969**, *187*, 828.
(38) Danley, W. J.; Mulay, L. N. *Mater. Res. Bull.* **1972**, *7*, 739.
(39) Houlihan, J. F.; Mulay, L. N. *Phys. Status Solidi B* **1974**, *61*, 647 and references therein.